Surface-engineered silicon nanocrystals

Nanoscale

RSC Publishing

FEATURE ARTICLE

Surface-engineered silicon nanocrystals

Davide Mariotti,*[a] Somak Mitra[a] and Vladimir Švrček*[b]

Cite this: *Nanoscale*, 2013, **5**, 1385

Received 15th October 2012
Accepted 5th December 2012

DOI: 10.1039/c2nr33170e

www.rsc.org/nanoscale

Quantum confined silicon nanocrystals (Si-ncs) exhibit intriguing properties due to silicon's indirect bandgap and their highly reactive surfaces. In particular the interplay of quantum confinement with surface effects reveals a complex scenario, which can complicate the interpretation of Si-nc properties and prediction of their corresponding behaviour. At the same time, the complexity and interplay of the different mechanisms in Si-ncs offer great opportunities with characteristics that may not be achievable with other nano-systems. In this context, a variety of carefully surface-engineered Si-ncs are highly desirable both for improving our understanding of Si-nc photo-physics and for their successful integration in application devices. Here we firstly highlight a selection of theoretical efforts and experimental surface engineering approaches and secondly we focus on recent surface engineering results that have utilized novel plasma–liquid interactions.

1 Introduction

Quantum confinement effects in nanoscale structures have attracted intense interest from the scientific community; theoretical, experimental and characterization efforts have all produced considerable progress which has allowed a greater understanding of quantum confined objects and has helped to envision their implementation in future technologies. The applications may impact upon the energy sector[1] as well as the health care sector[2–4] to mention just two.

Quantum confinement in semiconductor nanostructures is of particular interest and, depending on the materials, is generally observed for crystalline nanoparticles with diameters well below 50 nm and in most cases below 10 nm; quantum confined nanoparticles are generally called quantum dots or nanocrystals (NCs) to emphasize the crystalline nature that is required for specific quantum confined effects. The effect of quantum confinement is generally observed, for instance, in the widening of the bandgap[5] which is not generally perceived as a positive change in the materials properties; however the possibility of tuning the energy gap controlling the nanoparticle size is certainly an intriguing and exciting aspect for most

[a]*Nanotechnology & Integrated Bio-Engineering Centre-NIBEC, University of Ulster, UK. E-mail: d.mariotti@ulster.ac.uk*

[b]*Research Center for Photovoltaic Technologies, National Institute of Advanced Industrial Science and Technology (AIST), Tsukuba, 305-8568, Japan. E-mail: vladimir.svrcek@aist.go.jp*

Davide Mariotti received his PhD in 2002 from the University of Ulster (UK) in applied plasma physics. He worked internationally at the National Institute of Advanced Industrial Science and Technology-AIST (Japan) and at the Rochester Institute of Technology (Rochester-NY, USA). Since 2009, he has been Reader in Plasma Science and Nanoscale Engineering at the University of Ulster. His current research interests are in the fabrication and application of nanomaterials to energy harvesting and storage devices as well as a range of aspects that are related to plasma science and engineering.

Somak Mitra graduated at Dr Babasaheb Ambedkar Marathwada University (India). He then completed an MSc in Photonics (Erasmus Mundus) in 2010 and subsequently joined a PhD program at the University of Ulster in 2010, currently under the supervision of Dr Davide Mariotti.

researchers in the field. Another appealing quantum confinement effect is the increasing oscillator strength with decreasing size of the NP.[5] In other words NCs can be tuned to become "better" absorbers/emitters meeting very specific application requirements.

This has been largely confirmed for direct semiconducting materials such as II–VI and III–V materials whereby the synthetic capabilities have allowed the use of the corresponding NCs as models for verifying the theoretical predictions. With no doubts, direct semiconducting NCs have behaved up to the expected standard with notable results that go from theory[6,7] through synthesis[8,9] and applications.[10,11]

The indirect nature of silicon has however complicated this ideal scenario because different effects can be observed for direct and indirect transitions. The experimental observables originating from different phenomena can easily overlap providing a complex picture which is further aggravated by still limited synthetic capabilities.[12] Above all, silicon nanocrystals (Si-ncs) present highly reactive surfaces and it can probably be argued that the surface effects in Si-ncs have a stronger impact on the overall properties if compared with NCs made of other materials.[12] For instance significant differences are reported in the room-temperature photoluminescence (PL) of apparently similar Si-ncs obtained by different synthetic routes.[13] This is because surface characteristics result in strong variation of the PL wavelength and intensity.[5] It follows that the control of the surface characteristics is highly important and it is a challenge that needs to be overcome both for a clear understanding of the Si-nc properties as well as for their successful integration in application devices.

Given the range of difficulties encountered with Si-ncs, one might ask: why do we need to use Si-ncs? If scientific curiosity is not sufficient to answer this question we may want to consider the well-established infrastructure of Si-based technologies. This brings about know-how as well as considerable industrial investment to deal with raw materials, precursor supplies, processes and integration in existing device platforms. It has been shown for instance that Si-ncs can be integrated into flash memory devices with minimal disruption to conventional silicon technology.[14] The abundance, non-toxic nature† and limited environmental footprint of silicon should also be considered when Si-ncs are compared with other NCs.[6,12] Furthermore, the challenges presented by surface effects and the indirect nature of Si-ncs should probably be viewed as a great opportunity to provide tuning capabilities that are not achievable with other semiconducting NCs. The interplay of quantum effects and surface effects is highly visible in Si-ncs and calls for *surface* functionalization approaches that require *engineering* precision.

The need of surface engineering for Si-ncs has been well perceived by the research community with clear progress in a range of applications such as photovoltaics,[15–22] opto-electronic devices,[23,24] energy storage[25,26] and medical applications.[27,28] The "engineering" aspect of surface treatment is particularly important in consideration that functionalities require to be targeted to the specific applications and need to take into account almost pre-emptively the environment where the Si-ncs have to perform. This is to say that the optimal Si-nc surface requirements for a given application are likely to be detrimental for a different application. It should be noted that Si-nc success also depends on progressing with all other aspects of research including synthesis,[29–36] doping[37–46] and device integration such as for photovoltaics.[16–23,47–49] Only a cohesive and complete effort in all aspects of Si-nc research can lead to a full understanding of Si-nc properties and release the full potential of Si-nc application opportunities. While in this contribution our focus is on the surface engineering aspects, we fully believe that every scientific contribution in any of the research directions is equally important.

Control of surface characteristics is of paramount importance as surfaces play a key role in determining the properties, applicability and overall interactions of Si-ncs with the environment from synthesis and storage to applications. While all these aspects are fundamental, in this contribution we have given more emphasis to the interplay of surface effects with quantum confinement. The impact of surface characteristics on the overall Si-nc properties will be here briefly discussed summarizing results from theoretical calculations performed by a few different research groups; the intention is not to provide a full review but to highlight trends that are related to experimental surface engineering. Following, approaches to surface engineering will be described and in particular solution chemistry and plasma-based techniques will be briefly introduced. It should be noted that Si-ncs described as "free-standing" will be discussed here, which represent NCs that are neither grown on substrates (*e.g.* epitaxially) nor within a solid matrix. Both free-standing Si-ncs and Si-ncs supported within a solid matrix have advantages and application opportunities. For instance the synthesis directly in oxides, nitrides or amorphous materials can be easily integrated with processes already widely

Vladimir Švrček received his PhD in 2001 from the Charles University, Prague (Czech Republic) in Quantum Optics and Optoelectronics. He worked as a postdoctoral researcher at the French National Center for Scientific Research (CNRS), Strasburg from 2001 to 2005. Since 2005 he has been a researcher at the National Institute of Advanced Industrial Science and Technology-AIST (Japan) in the Research Center for Photovoltaic Technologies. Currently, his main research interest lies in the development of advanced technologies of silicon-based quantum nanostructured thin film multiexciton solar cells as well as aspects that are related to the novel physical phenomena of next generation solar cells.

† The non-toxic nature is intended in terms of silicon as a chemical element while in general for nanoparticles of any material, the research still needs to provide exhaustive and complete answers.

used by the microelectronic industry.[36,50–52] A carefully selected embedding material can offer advantages also for carrier mobility in given applications such as for photovoltaics.[36,51] On the other hand, free-standing Si-ncs offer the possibility to vary the compressive strain at the surface, while embedded Si-ncs are necessarily always strained;[50] this has consequences on the Si-nc optical properties.[50,53] Importantly in the context of surface engineering, the presence of the matrix can limit the access and modification of Si-nc surface characteristics. For this reason, in this contribution the focus will be on unsupported Si-ncs (*i.e.* free-standing) because effectively 3-dimensional surface engineering is not applicable to Si-ncs embedded in solid matrices or grown on substrates. Finally, we will discuss our recent advances that are related to surface engineering by "*Plasma-induced Liquid Chemistry*" (PiLC) which brings together some of the advantages of solution chemistry with the indispensable non-equilibrium chemistry of plasma processes. The opportunities offered by PiLC will be exemplified by laser-produced plasmas in liquid as well as plasma–liquid interactions induced by gas-phase electrical discharges. These techniques have been used to modify the surface characteristics of Si-ncs with drastic changes in the opto-electronic properties.

2 The interplay of quantum confinement and surface effects

2.1 Theoretical considerations on the distinctive nature of silicon nanocrystals

As a model to understand the basic distinctive properties of Si-ncs, hydrogen-based terminations are often considered at the surface of the NCs. As the size of the Si-ncs is reduced, similarly to the "particle in a box" where the separation of the energy levels is increased, the bandgap of the Si-ncs is also expected to increase.[5] While this is true for the indirect bandgap, the complexity of the energy structure at the direct bandgap leads to an opposite result and the energy gap is actually expected to decrease (from 3.32 eV) with increasing quantum confinement.[54] In bulk silicon the direct bandgap is virtually a transient energy level as electrons can relax towards the minimum of the conduction band at the indirect bandgap in a sub-picosecond timescale.[54,55] It is clear that with an increasing indirect bandgap and a decreasing direct bandgap the energy barriers and probabilities of the different transition mechanisms are drastically affected with dramatic consequences on relaxation paths of electrons at the direct bandgap minimum.

At the same time, the indirect transitions that generally require the intervention of phonons are also highly affected by quantum confinement. As the size of the Si-nc becomes comparable to the Bohr radius (~4.5 nm),[13] an increasing constraint is imposed to the wave function of the carriers so that, due to the Heisenberg principle, the momentum conservation is relaxed. Or in other words, the position of carriers in *k*-space is less defined and therefore carriers can transit from energy levels at different points of the Brillouin zone with no need for energy-matching phonons. This results in a "direct-like" behaviour for Si-ncs whereby indirect transitions can occur with a higher probability than in bulk silicon.

Another consequence of quantum confinement is the so-called "phonon bottleneck" which originates from an overall decreasing density of states and increasing separation between individual levels. If in bulk silicon hot electrons can easily relax to lower energy levels by releasing phonons, the modified density of states with larger gaps can limit (by one to three orders of magnitude) the electron relaxation through heat release.[54] The consequence of this is that the dynamics of the different mechanisms is highly affected because the lifetime of carriers in this case is increased. One of the mechanisms that can benefit from a re-organization of the transition dynamics is carrier multiplication (CM). This is a particularly interesting feature of Si-ncs that is related to the effect of quantum confinement on the impact excitation process. In this process, a high-energy photon initially generates a high-energy exciton. The high-energy exciton can then relax following different relaxation channels; in quantum confined NCs, the probability for the exciton to relax through the generation of other excitons is high compared to the bulk case. Therefore multi-exciton generation (MEG) becomes a preferred relaxation channel because quantum confinement drastically reduces electronic screening and enhances Coulomb interactions between electrons and holes due to their close proximity.[6,56–58] Highly efficient MEG was initially reported for environmentally unfriendly II–VI compounds such as PbSe and CdTe and has now been observed also for Si-ncs.[56] Another analogous CM mechanism is the so-called space-separated quantum cutting (SSQC).[15] While MEG is due to the Auger interaction of multiple excitons within the same NC, in SSQC the multiplication process occurs across different but neighbouring Si-ncs. The energy transfer in SSQC is accompanied by the relaxation, in the NC where it originated, from a highly excited state toward the lowest-energy excited state.[56]

From an experimental point of view, all this means that when probing the properties of Si-ncs, clear differences are observed compared to bulk silicon. Firstly, on reducing the size, the excitonic emission intensity of Si-ncs is largely increased and blue-shifted (for H-terminated Si-ncs). However understanding the origins of the experimental observations remains complicated and both time-/temperature-dependent measurements are often required to provide some additional valuable information.[13] Although the general theoretical descriptions are found to agree with experimental results, there is still much debate at a more detailed level, which is further complicated by the considerable gap between "theoretical Si-ncs" and "experimental Si-ncs". The theory–experiment gap is in part due to computational limits on one side and synthetic/characterization limits on the other, *i.e.* while theoreticians find it difficult to calculate properties of NCs with diameters larger than 1–2 nm, the experimental capabilities have difficulties in producing and characterizing high quality samples with sizes below 3 nm. It may be useful to point out that a 1 nm diameter NC (which may be regarded as a "cluster") is formed by about 40 atoms[13] and consequently might lack the required extended crystalline structure to extrapolate the computational results to larger size NCs. It will be shown here below that clusters often exhibit strong fluctuations in the calculated bandgaps due to

drastic re-structuring when the number of atoms (*i.e.* the cluster size) is changed. The other item contributing to the theory–experiment gap is the surface of the Si-ncs. However the computational efforts are increasing to address this issue and several reports can now be found in the literature about Si-ncs with a range of different surface characteristics.[59] A selection of these results will be briefly overviewed in the next section.

2.2 Comments on theoretical efforts to predict surface effects

Quantum confinement is a key factor, but because there can be a high relative percentage of silicon atoms at the surface (up to 100% in a Si_{10} cluster with a diameter of ~0.7 nm), the role of surface states is likely to be important.[60] Therefore surface characteristics can have a strong influence on the overall properties and behaviour of Si-ncs, which can generally be observed in profoundly modified optical properties.[61] The typology of surface characteristics includes both the chemical composition (*e.g.* Si–H *vs.* Si–O–H, *etc.*) and the quality of surface bonds where strains can play a considerable role.[53] Two fundamental mechanisms are responsible for surface effects:

(a) The wave functions of carriers are delocalized over the NC volume to include its surface; this results in the energy structure that is influenced by the surface states (and beyond). Also, ligands that are passivating the Si-nc surface contribute somewhat to the state density. Therefore, the optical properties are sensitive not only to the size of the particles but also to the surface chemistry, network distortion, and geometry of the structures.[13] It follows that this type of surface effects are generally stronger in small Si-ncs (<3 nm diameter) and, while still observable, tend to fade out as the diameter is increased.

(b) The second mechanism is due to the small volume of Si-ncs which allows for carriers to easily diffuse into/from the NC's core/surface; for instance while excitation photons may be absorbed in the core, surface-localised states may facilitate the recombination processes and therefore either the emission intensity and/or its wavelength are affected.[61] The result is that the NC morphological structure and the surrounding matrix optical properties also influence the luminescence process.[13] This mechanism acts therefore on the transition dynamics and, while being still sensitive to the size of the NCs, generally persists in larger NCs (>3 nm)[62] depending on the specific surface chemistry.

It should be noted that while the first mechanism directly induces changes in the energy structure of the Si-ncs, the second mechanism is acting through a modified relative distribution of transition probabilities; from this observation it should be expected for the first mechanism to be size-dependent while the second, in principle, should be less sensitive to changes in the Si-nc size. However, the interplay of all mechanisms does affect the efficiency of surface-based recombination and therefore the size indirectly affects transitions at the surface. CM is one of the phenomena to be influenced by surface characteristics as surface ligands with their vibrational states can contribute to phonon-assisted MEG.[6] Overall surface effects in combination with quantum confinement and the possibility of competing direct/indirect transitions make the interpretation of experimental observables rather complex. This is in consideration also that the available assessment parameters are often limited and it is often required to analyse in detail the decay rates of the luminescence processes. Fast decay rates were suggested to involve surface defects, molecular-like traps, or shallow states, as carriers generated in the core are rapidly localized in the lower energy surface states from which the particle emits.[13] For these reasons theoretical work is fundamental to bridge and complement the experimental results.

In the analysis of surface effects, the H-terminated Si-nc is generally considered as a reference model to understand the very basic fundamental photo-physics resulting from surface modifications. Surface terminations based on Si–H and Si–C bonds have not shown considerable differences in the bandgap (~0.2 eV) and therefore absorption features have been found for the most part to be invariant.[12] The length and type of organic chains have also been found to have little influence in determining the bandgap as long as terminations are through the Si–C bonds.[60] However the replacement of hydrogen atoms with alkyl groups or other organic terminations in Si-clusters considerably varied both the above-band-edge optical absorption and the energy levels with respect to the vacuum of the highest occupied molecular orbital (HOMO) and of the lowest unoccupied molecular orbital (LUMO).[12,56,60] The new absorption features have been associated with localized states at the Si–C bonds or in the organic chain.[56] Although the bandgap remained unchanged, the electron affinity of the clusters was drastically affected with possible consequences on the Si-nc surface charge distribution: the surface hydrogen atoms are negatively charged in hydrogenated Si-ncs while they are positively charged in alkyl-terminated Si-ncs.[12] This results from the electro-negativity index being ~1.9 for silicon, ~2.1 for hydrogen and ~2.5 for carbon[12] with practical implications for using Si-ncs in colloids and for their employment in many applications. Interesting and related aspects also originate from the steric effects of longer organic terminations which can affect the overall cluster structure stability and formation energies. In summary, the Si-nc bandgap is not drastically affected in these cases and excitons do not find the Si–H or Si–C interface bonds to be preferential recombination channels. Therefore absorption and photoluminescence experiments may produce similar results and would be insufficient to discriminate between Si-ncs with Si–C or Si–H surface bonds.

The picture is very much modified if Si–O bonds are present at the Si-nc surface.[60] Generally the presence of Si–O bonds induces a reduction in the optical bandgap. At the same time, possibly due to the oxygen electro-negativity index (~3.4), recombination at the surface is highly probable so that the two mechanisms (a) and (b) previously described tend to produce overlapping effects. For instance, it has been shown by R. Guerra *et al.* that the replacement of H-terminations with OH terminations in Si-clusters (10–90 atoms with ~0.7 to 1.5 nm diameter) produces a consistent bandgap reduction with differences close to 3 eV for the smallest number of atoms (Fig. 1).[53] Larger hydrogenated clusters with 1.5 nm diameter presented a bandgap of ~2.5 eV while the corresponding

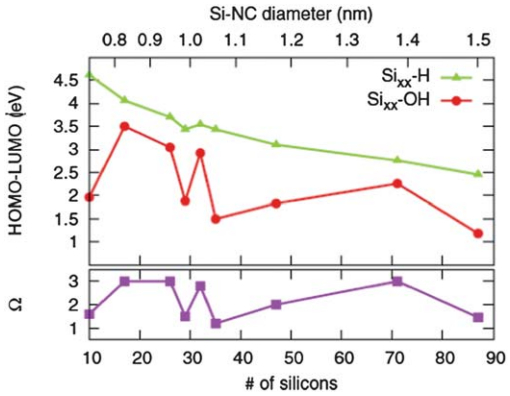

Fig. 1 Gap between the highest occupied molecular orbital (HOMO) and the lowest unoccupied molecular orbital (LUMO) for the hydroxide (circles) and hydrogenated (triangles) nanocrystals; the corresponding average number of Si–OH bonds per surface silicon atom Ω (squares) is shown at the bottom. Reprinted with permission from ref. 53, copyright 2009 American Physical Society.

OH-terminated Si-clusters had a much smaller bandgap close to 1 eV (Fig. 1).[53] However it should be mentioned that hydroxide clusters are strongly dependent on the actual surface configuration where the average number of Si–OH bonds per surface silicon atom (Ω in Fig. 1) can induce large bandgap shifts. Specifically, clusters with silicon atoms that were on average bonded to a higher number of oxygen atoms (*e.g.* Si–Si≡$(OH)_3$) had been shown to present larger bandgaps compared with Si-clusters with surface silicon atoms bonded on average to a lower number of oxygen atoms (*e.g.* Si_3–Si–OH).[53] As a result, the bandgap trend with increasing quantum confinement was still present but modulated by varying surface characteristics and arrangements (see Fig. 1).[53]

One might expect that at larger NC sizes (closer to the 3–5 nm diameter range), as the surface curvature is reduced, the bandgap fluctuations (red circles in Fig. 1) due to surface restructuring are minimized.[63] The reduction of the bandgap fluctuations may also be ascribable directly to a reduction of the variations of the value of Ω for increasing sizes. Extrapolating the results of Fig. 1, the difference in the bandgap between hydrogenated and hydroxide Si-ncs should be still observed for larger and more experimentally available Si-ncs. An interesting observation was that the interface properties and specifically the surface silicon bonding seemed to have a larger effect than any embedding matrix around the Si-ncs. This was shown by comparing the absorption properties of Si-ncs embedded in a silica matrix with free-standing Si-ncs terminated with strained Si–OH bonds.[53] The two types of Si-ncs presented almost identical absorption features indicating that the oxide matrix contributed to changes in the Si-nc properties only through induced strain at the Si-nc–oxide-matrix interface. However, from an experimental point of view, the presence of the matrix may complicate the assessment of Si-nc fundamental properties as the oxide itself can produce for instance absorption and emission features.[53,64]

Surface terminations that are based on Si–O bonds (including Si–OH) all exhibit considerably lower bandgaps when compared with bandgaps of the corresponding hydrogenated Si-ncs. At the same time, D. König *et al.*[65] showed that differences between different Si–O bond arrangements existed. The bandgap of very small OH-terminated Si-clusters (~0.7 nm diameter) increased when an oxygen bridge bond (*i.e.* Si–O–Si) replaced only one of the OH-termination.[65] An interesting feature was that Si–O–Si bridge bonds exhibited higher charge transfer compared to the Si=O or Si–OH terminations.[65] The replacement of the full Si-nc surface with bridge bonds would be expected to bring more drastic differences between clusters with different Si–O bond configurations because as the polarity of the Si-nc interface increases, the optical bandgap becomes increasingly affected by charge transfer at the interface rather than by quantum confinement.[60] These considerations suggest opportunities for tailoring Si-nc properties with different oxygen-based surface arrangements. For Si-ncs embedded in an oxide matrix[66] and indeed for extended or flat silicon/oxide interfaces,[67] preferential Si–O bonds may exist (*e.g.* Si–O–Si); in these cases it is therefore more difficult to control the surface characteristics also in consideration that most often highly energetic annealing processes are required for the formation of Si-ncs.[66] In contrast, free-standing Si-ncs that are amenable to post-synthesis surface engineering can rely on non-equilibrium and/or kinetically driven surface reactions where different bonding arrangements may become available. Some of these opportunities will be discussed in Section 3, nonetheless it should be noted that highly controlled surface engineering techniques as well as in-depth characterization studies will be required to fully unveil these aspects.

Silicon back-bonds are experimentally observed to be easily oxidized and therefore the effects of back-bond oxidation are also very important. Because of drastically different bonding arrangements within a few atom layers, the initial oxidation steps can introduce strong variations in the properties of Si-ncs compared to non-oxidized Si-ncs (assuming the same core size); such changes are progressively less pronounced as the oxide extends to a thicker and thicker shell (still assuming the same core size). For instance the HOMO–LUMO gap of an H-terminated Si_{17} cluster reduces from 4.17 eV to 3.39 eV when a back-bond oxide layer is added (Si_{17}–$O_{36}Si_{24}H_{60}$) and reduces only to 3.25 eV when a double oxide layer (Si_{17}–$O_{96}Si_{66}H_{108}$) is introduced.[68] However, the oxidation process generally "eats up" the silicon core and in such cases the effect of quantum confinement dominates so that the gap increases, for example from 3.22 eV (Si_{41}–H_{60}) to 3.39 eV (Si_{17}–$O_{36}Si_{24}H_{60}$) and to 5.13 eV (Si_5–$O_{48}Si_{36}H_{60}$). Anyhow, it is important to note that OH-terminations are still much more effective in reducing the gap of silicon clusters compared to back-bond oxidation whereby the gap of Si_{17}–$(OH)_{36}$ is calculated to be 2.99 eV compared with that of $Si_{17}H_{36}$ (4.17 eV); this is due to the localization of the LUMO state induced by the isolated OH oxygen atoms *versus* a more distributed charge density in Si-ncs with back-bond oxide where oxygen atoms present increased interactions.[63,68]

The quantitative comparison of different theoretical results remains quite difficult as different values for bandgaps and energy levels are often produced. The differences are due to the use of different computational techniques, calculation frameworks as well as the emphasis given to different physical aspects

such as structural configurations, strain, *etc.* However, by comparing the qualitative nature of the terminations depicted above (with hydrogen, carbon and oxygen), a clear trend can be noticed: "core-induced" quantum confinement effects are stronger in Si-ncs with low electronegative terminations while the surface effects take over when terminations exhibit higher electronegative index. It may be noteworthy to point out that, despite the complications arising from the additional strain fields, the same statement generally holds in Si-ncs embedded in insulators.[69,70]

This trend can be exemplified by analysing the results of a theoretical study of E. Ramos *et al.* which compared –H, –Cl and –F terminations.[71] This type of surface states have the advantage of isolating the effect of electro-negativity considering that steric hindrance (found in organic long chains or even in –OH terminations), Si–Si back-bond strains effects (*e.g.* in Si=O or Si–O–Si) and the electron affinity effect of additional atoms (*e.g.* Si–NH_2) are minimized. Fig. 2a presents the results from a study of E. Ramos *et al.* (see Table 2 in ref. 71) and plots the HOMO and LUMO energies *versus* the electro-negativity of the termination (hydrogen, chlorine or fluorine) for a Si_{35} cluster.

It is clear that both the LUMO and HOMO are affected by the electronegative character of the terminations, with the LUMO being strongly modified. Therefore the electron affinity, surface charging and many practical properties of Si-ncs are affected. Importantly, because the LUMO energy level is more sensitive to the termination's electro-negativity, the bandgap is also reduced as the electronegative character is increased. Furthermore a high electronegative character tends to take over any "core-induced" quantum confinement effect clearly emphasizing the interplay of different types of mechanisms. This is shown in the bandgap values calculated by E. Ramos *et al.*[71] for clusters of different sizes terminated by hydrogen or fluorine (Fig. 2b). It can be easily noticed that hydrogen with a low electro-negativity index allows for core-induced quantum confinement to exhibit the size-dependent bandgap properties while fluorine-terminated surfaces dominate the influence on the Si-nc electronic structure. As the size of the Si-ncs is increased the difference between the core-induced and surface-induced bandgap is reduced however it may be still considerable for application-relevant dimensions. Finally, although a fully quantitative comparison is not possible, it can be observed that the results previously discussed on C-terminated or O-terminated Si-ncs are justified by their electronegative character: carbon presents characteristics similar to those observed for hydrogen while oxygen (~3.4) sits between chlorine (~3.2) and fluorine (~4.0). As previously mentioned the complexity and intervention of a range of factors make the interpretation of experimental results a lot more complicated, in particular for oxygen-based surfaces where a wide range of bonding arrangements is possible.

In summary theoretical calculations can provide valuable details for the energy level re-distribution in Si-clusters/-ncs under different conditions, *i.e.* type-(a) mechanisms. However, theoretical efforts to produce the interpretation of type-(b) mechanisms, *i.e.* transition dynamics and time-dependent descriptions, are still limited.[6]

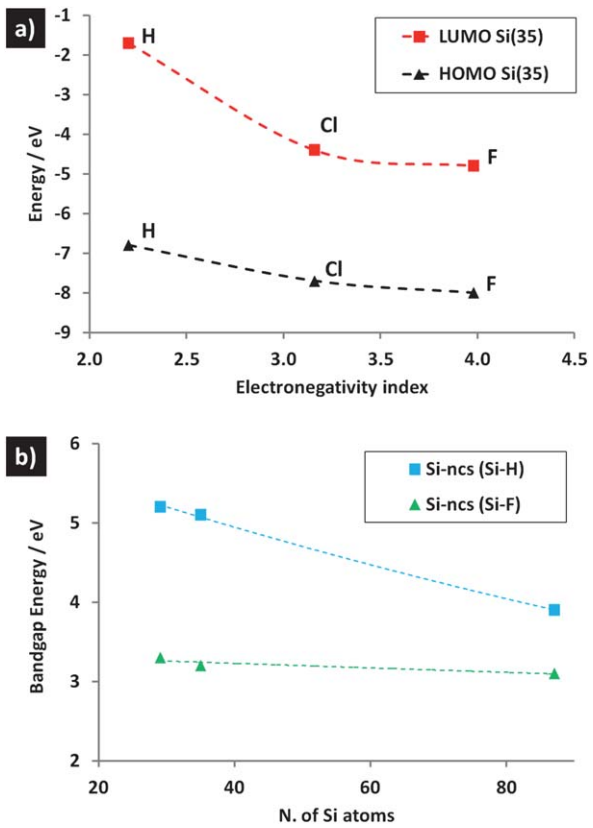

Fig. 2 (a) Highest occupied molecular orbital and lowest unoccupied molecular orbital levels for Si-ncs terminated with –H, –Cl and –F; the *x*-axis shows the electro-negativity of the terminating atom. (b) Calculated bandgaps for H- and F-terminated silicon nanocrystals for different cluster sizes. Both plots report tabular data published by E. Ramos *et al.* (see Table 2) adapted with permission from ref. 71. Copyright (2012) American Chemical Society.

3 Silicon nanocrystal surface engineering by plasma–liquid interactions

3.1 Introduction to Si-nc surface engineering

The selection of the synthesis approach and the choice of the corresponding precursors can be considered part of the surface engineering process. For instance, plasma-based synthesis utilizing silane precursors is known to provide Si–H terminations[29–31,72] while the use of a $SiCl_4$ precursor for both plasma- and solution-based syntheses terminates the Si-ncs with chlorine.[30,31,73,74] A recent report has also shown the possibility of solution-based synthesis of Si-ncs leading to $C_xH_yNH_2$ terminations.[32] Post-synthesis surface engineering of Si-ncs has so far largely relied on traditional or enhanced (*e.g.* thermally, by illumination) solution chemistry[33,73,75–81] and only very recently, alternative approaches have made significant and very promising advances.[17,22,23,75,82–89]

The solution chemistry approach is generally achieved through the realization of a chemically active surface (*e.g.* Si–Br, Si–Cl, Si–OH, Si–H), which allows further modification. In the last decade photochemically initiated hydrosilylation has found wide application.[59] Photochemical and thermal hydrosilylation

of Si surfaces is a free-radical mechanism *via* homolytic cleavage of a hydride bond. The proposed mechanisms describe complex relationships among the wavelength of irradiation and the alkene or alkyne species attached that determine the functionalization of Si surfaces.[90] On the other hand, it has been reported that the dangling bonds and the reconstructed bonds at the Si-nc surface could be passivated and transformed with deuterium (D) and ND_x by using deuterated ammonia (ND_3), with considerable effects on the optoelectronic properties of Si-ncs.[89] Deuteride and ND_x surface passivation allows enhancement of PL intensity if Si-ND_2 species are predominantly adsorbed onto the Si-nc surface. It is likely that nitrogen-containing radicals (ND_2 and ND) in the strained Si–Si reconstructed bonds lead to N atoms in a bridge configuration (*i.e.* Si–N–Si).

Although debate still remains on the chemical pathways leading to stable surface chemistries, surface engineering of Si-ncs by solution chemistry remains an established technique. These techniques can rely on considerable know-how and transferrable expertise from a range of different nanoparticles; furthermore these approaches allow the use of Si-ncs directly in liquids which is advantageous for many applications. At the same time the organic long-chain terminations provided by some of these techniques are a limiting factor for the Si-nc electrical properties as required for opto-electronic devices.[91] Also, the process chemistry required to achieve Si-nc surface engineering and remove by-products can be in some cases very time-consuming.[91] For these reasons research efforts are being made towards alternative processes capable of Si-nc surface engineering. Some of these efforts have utilized gas-phase and continuous-flow plasma/thermal processes which have been highly successful for other materials;[92] for example, plasma-synthesized Si-ncs were flowed directly after synthesis into a furnace for the thermal activation of organic ligands.[93] Following these results, continuous-flow processes that combine two consecutive plasma reactors have also been investigated;[17,23,83] the replacement of the thermally activated surface engineering step with a plasma-based step has several advantages as hot plasma electrons are highly effective in dissociating precursors which can provide non-thermodynamic pathways and highly reactive species.

A double-plasma system has been used to functionalize Si-ncs in the gas-phase with a range of organic-based terminations.[91] These organic-grafted Si-ncs were found to be highly soluble in non-polar solvents; however the optical properties could be improved only after an annealing step. The same group demonstrated improved hydrogen passivation utilizing a silane plasma for the synthesis of Si-ncs followed by hydrogen gas injection at the exit of the synthesis plasma.[83] In this case, the secondary plasma was not used and the afterglow reactive chemistry was instead sufficient for surface engineering *via* hydrogen radicals.[83] The same system was then used to inject aerosols of organic precursors in the afterglow of the synthesis-plasma; the Si-ncs produced and surface engineered with this method were successfully integrated into light-emitting devices showing that the electrical interface properties were satisfactory.[23] Synthesis and surface engineering in double plasma configurations are powerful approaches that can offer a range of opportunities. Uchida *et al.* have explored the possibility of using different gas precursors for surface engineering in the secondary plasma and have successfully provided nitrogen-based terminations for Si-ncs.[17] There is no doubt that reactive non-equilibrium plasmas can offer more opportunities in the future for gas-phase surface engineering of Si-ncs; in particular oxygen-based passivation *via* oxygen radicals and kinetic-driven surface reactions[94] may lead to superior control of the Si–O bonding configurations.

3.2 Laser-produced plasmas and electrical discharge plasmas in contact with liquids

The possibility of working with Si-ncs in colloids is very attractive for a range of reasons that include ease of storage as well as processing *via* low-cost techniques such as screen printing and spray coating. In some cases, such as for medical applications, it is a requirement for Si-ncs to be supplied and used in liquids. We have therefore explored possible techniques for Si-nc surface engineering directly in colloids; the aim is to achieve a better control of the surface chemistry and also to search for new surface engineering opportunities beyond the traditional wet chemistry. In this sense coupling plasmas with liquids seemed to be a promising option where the non-equilibrium kinetically driven chemistry activated by plasmas could be transferred to a liquid environment. We have investigated three different approaches as depicted in Fig. 3. In all cases the colloid is formed by Si-ncs dispersed in liquid media (*e.g.* ethanol or water).

The first technique employs a pulsed laser that produces a plasma plume within the colloid (Fig. 3a). Different types of lasers can be used,[19,21,34,82,95] however for the specific purpose of surface engineering a Kr:F laser was generally used (245 nm, 20 Hz, 130 mJ per pulse).[22] The process takes place at room temperature for different time durations from a few minutes up to a few hours. The laser beam is focused onto a 3 mm diameter spot on the liquid surface by a lens with a focal length of 250 mm. During the irradiation, the glass container is closed and rotated. This laser-based process combines the benefit of multiple processes that include photothermal heating and

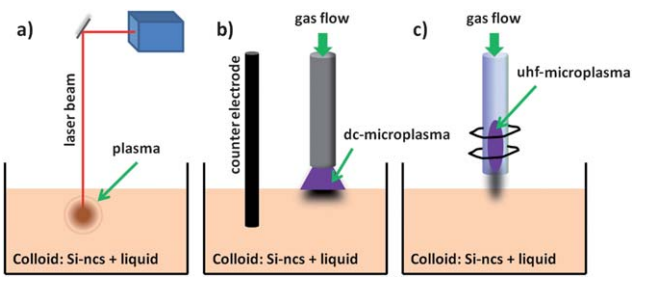

Fig. 3 Schematic diagram representing three different plasma–liquid systems for surface engineering of nanomaterials and specifically for silicon nanocrystals (Si-ncs): (a) a laser beam is used to generate a plasma in the liquid; (b) an atmospheric pressure direct-current (dc) microplasma is generated outside and coupled to the colloid *via* a counter electrode; (c) an ultra high frequency (uhf) microplasma is generated in a quartz capillary and "jetted" out onto the colloid.

Coulomb explosion.[96] The chemistry induced on the surface of the Si-ncs depends on the type of the liquid and in general it also depends on both the laser-induced heat as well as the production of a range of radicals such as hydroxyl groups.

The second approach relies on the generation of a direct-current (dc) atmospheric pressure plasma between a metal tube-electrode (nickel or stainless steel and typically with 0.7 mm or 0.25 mm internal diameter) and the surface of the colloid (Fig. 3b). A counter electrode (made of a carbon rod or a metal wire) is immersed about 5 mm in the solution at a distance of about 2 cm from the metal tubing. Pure He or Ar gas is flowed at a rate of 25–100 sccm in the tubing to supply the plasma gas. The distance between the surface of the colloid and the end of the metal tubing is set initially at 0.5–1 mm; however the distance tends to increase due to the evaporation of the liquid. In order to sustain the plasma, a constant current is applied for each surface engineering process and for different processing conditions the current has been varied between 0.5 mA and 5 mA. The initial required voltage to sustain the constant current can be as high as 2 kV but it is progressively decreased down to ~500 V. We have verified that the main parameters affecting the outcome of the treatment are the processing current, the Si-nc concentration and the solution of the colloid; in particular the current and the Si-nc concentration determine the process rate while the solution is mainly responsible for the type of induced surface chemistry. The other parameters such as capillary diameters, gas flow, *etc.* (within the ranges described above) have been found to have very little or no influence on the results of the process. Although this technique is relatively new, there has been some good progress in the understanding of the plasma–liquid interactions.[86–88,97–100] The main feature of this set-up is that electrons "injected" from the plasma are the main source of induced liquid chemistry.[88,99,100] The interaction of plasma-electrons with the colloids is then responsible for the cascaded liquid chemistry that contributes to surface engineering of the Si-ncs. It should be mentioned that this technique is also used for both the synthesis and surface engineering of a range of other nanomaterials.[31,86–88,97,98,101] One of the drawbacks of this technique is that the colloid needs to be somewhat conductive; the set-up shown in Fig. 3c has recently been developed in part to overcome this limitation of the dc-microplasma shown in Fig. 3b.

In the set-up shown in Fig. 3a and c, a counter electrode is not required as the atmospheric pressure microplasma is in this case generated within a quartz capillary (0.7 mm internal diameter) using external copper ring-electrodes about 3 mm apart; the plasma "jet" exiting the quartz capillary is then put in contact with the surface of the colloid. An extensive range of configurations, processing conditions and excitation approaches can be used for this purpose; we will here describe the conditions that are specifically related to the results reported below. Pure helium was flowed at a rate of 250 sccm and an ultra high frequency (uhf; 450 MHz) power supply was used to sustain the microplasma (60 W as recorded at the power supply). The distance between the end of the quartz capillary and the surface of the colloid was initially adjusted to about 2 mm; however also in this case the distance increased with processing time due to evaporation. The chemistry produced with this type of plasma can be quite different compared to the dc-configuration shown in Fig. 3b; however our results have shown so far very similar effects on the Si-ncs so we believe that also in this case the plasma-electrons play a dominant role.

The three techniques described above have been used for the synthesis and surface engineering of several nanomaterials (Si-ncs, Au-, Ag-, $BaTiO_3$-nanoparticles, graphene, carbon nanotubes, *etc.*)[19,31,34,86–88,97,98,102] and a much wider range of materials and applications are possible.[103,104] Here we will focus however only on the surface treatment of Si-ncs that have been pre-synthesized by electrochemical etching and dispersed either in water or ethanol. For the electrochemical etching process, similarly to our previous work,[105] we have used p-type boron-doped silicon wafers (⟨100⟩, 0.1 Ω cm, thickness 0.525 mm). In order to collect the Si-ncs, these are mechanically removed or essentially "scratched" from the wafer surface. The process produces a dry powder of Si-ncs with a diameter of 3–5 nm which generally includes Si-nc aggregates of different sizes up to the micrometer range. The powder is then stored in glass containers under ambient conditions and exposed to air. It is important to highlight that for most applications, aggregated Si-ncs are not desirable and indeed do not facilitate the surface engineering process because the interface between aggregated Si-ncs is not accessible to any type of surface chemistry. Mechanical pulverization in part allows formation of single and non-aggregated Si-ncs, however these need to be separated from the other aggregates in the powder. Different methodologies have been applied to fragment and/or filter Si-ncs produced by electrochemical etching including sedimentation, ultra-sonication, filtration, centrifugation, laser fragmentation and any combination thereof. Alternatively synthesis techniques that produce Si-ncs bottom-up (*e.g.* plasmas[29–31,72,74]) should be considered. In our work we have used sedimentation to eliminate larger Si-nc aggregates; although this approach has some limitations, it has allowed us to demonstrate the potential of plasma–liquid surface engineering. Therefore, before any type of surface engineering process, ~3 mg of the powder is dispersed in 10 mL of ethanol or water, and only the supernatant part is collected after >15 minutes of sedimentation. Surface engineering has been applied always within one hour from dispersion of the Si-ncs in water or ethanol.

We have previously studied in detail the characteristics of these Si-ncs both as dry powder as well as in colloids in water or ethanol.[87] The dry Si-nc powder presents very constant characteristics for an extended period of time (≫ months) with stable H-terminations and a degree of oxidation which does not vary over time.[87] The dry powder exhibits strong room-temperature photoluminescence (PL) that peaks in the range 590–620 nm (2.0–2.1 eV) depending on the storage conditions. However, the dispersion of the Si-nc powder in water initiates a slow and low-temperature oxidation process which has detrimental effects on the optical properties of the Si-ncs (see blue diamonds in Fig. 5).[87] Specifically, contact with water leads to a decrease of the Si-nc size in favour of a growing oxide shell which leaves behind defects and highly strained bonds. Depending on the storage conditions, within a few days the Si-ncs have lost most

of their PL and exhibit a blue-shifted weak peak just below 580 nm (~2.1 eV). Dispersion of the Si-ncs in ethanol follows an identical pattern but with much slower oxidation rates.[87] We will show in the next sections that the plasma–liquid approaches depicted in Fig. 3 can be used to modify the surface characteristics of Si-ncs and prevent degradation of the optical properties achieving stable photoluminescent Si-nc colloids both in water and in ethanol.

3.3 Surface engineering by short pulsed laser-based processing

Laser-based surface engineering in liquid media depends on multiple mechanisms which have different time-scales and effectively leave a relatively narrow processing window. This mostly depends on ablation intensity and laser processing time[22] leading to the formation of shock waves and to photothermal heating.[96] In particular, shock waves in the colloid can produce the fragmentation of Si-nc aggregates by the detachment of the Si-ncs that are most weakly attached to them.[106] Our investigations showed three different processing timeframes occurring during laser processing[22] as a result of the combined fragmentation–surface engineering process.[22] It follows that Si-ncs with different characteristic properties can be observed at subsequent times; the photoluminescence spectra of Si-ncs at the start of the laser-based process (0 min) and following 15 min and 35 min processing are shown in Fig. 4a. In the initial phase (0–15 minutes processing), Si-ncs experience a surface restricted passivation by laser-produced radicals, most notably OH groups, which reduces surface defects and increases the PL intensity by about 30% (see the corresponding changes in the spectra from 0 min to 15 min in Fig. 4a). It should be noted however that the PL increase is possible, thanks also to the fragmentation of aggregates which allows a larger number of single Si-ncs to be fully passivated. We attributed the ~0.07 eV red-shift (from ~2.09 eV to ~2.01 eV or from ~593 nm to ~616 nm) to the replacement of H-terminations with Si–OH bonds as supported by theoretical calculations (see above) and by our Fourier transform infrared spectroscopy.[22] Si–OH bonds are also prone to condensation to form an oxide layer.[107] After 15 min processing, with stable oxygen-based ligands at the Si-nc surface, oxide growth is likely to proceed at the Si–Si back-bonds or at any remaining $(SiH)_2$ groups, *i.e.* Si-dimers, which present strained angles and therefore are susceptible to water cleavage.[107] This slow oxidation process is however introducing further defects[107] leading to deterioration of the PL properties, see changes in Fig. 4a from 15 min to 45 min. The PL intensity decrease is accompanied by a small blue shift that may indicate a reduced core in favour of a growing oxide shell;[22] as previously discussed the effect of core-induced quantum confinement is masked by stronger oxygen-based surface effects[62] and the blue shift is therefore rather small.

This analysis highlights that effective oxygen-based surface engineering can be achieved by laser processing and that this occurs within the initial phase, *i.e.* <15 min processing time for this specific power (130 mJ per pulse). During this processing window, also the fragmentation process is effective contributing to a high number of Si-ncs being exposed to 3-dimensional (3D) surface engineering.

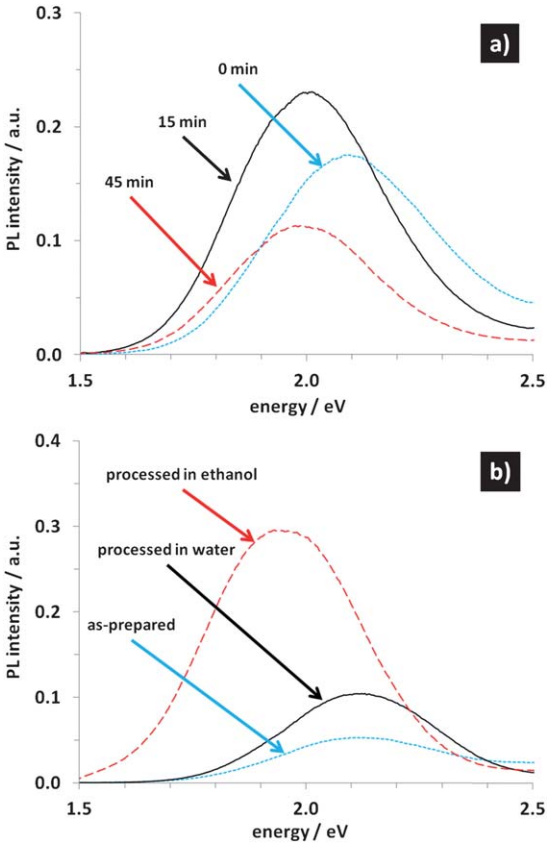

Fig. 4 (a) Typical photoluminescence (PL) spectra evolution from silicon nanocrystals (Si-ncs) after nanosecond laser processing in water at different times. (b) PL spectra of as-prepared silicon nanocrystals (Si-ncs) dispersed in water and after laser-based surface engineering (~12 min) in different liquid media (water or ethanol). The excitation wavelength was 400 nm for all samples.

The laser process conducted in water can be compared with the same process in ethanol. Fig. 4b shows the PL spectra of surface-engineered Si-ncs in water and in ethanol by ns laser processing. A higher PL intensity and a clear red shift are observed when laser processing is done in ethanol. The surface-restricted oxidation attributed to OH radicals is more efficient in ethanol and the surface engineering processing window is also greatly increased (not shown here) so that the slow inward oxide growth is virtually suppressed in ethanol if compared with processing in water (*i.e.* processing for >15 min in Fig. 4a).

3.4 Microplasma surface engineering in water and ethanol

Fig. 5 summarizes the photoluminescence properties of Si-ncs that have been surface engineered by the microplasma processes shown in Fig. 3b and c, *i.e.* processed by dc-microplasma (both in water and in ethanol) and processed by uhf-microplasma (in water only) respectively. For reference, the optical properties of Si-ncs stored in water for the same time are also reported.

All the surface engineering processes have stabilized the optical properties of the Si-ncs and prevented the degradation

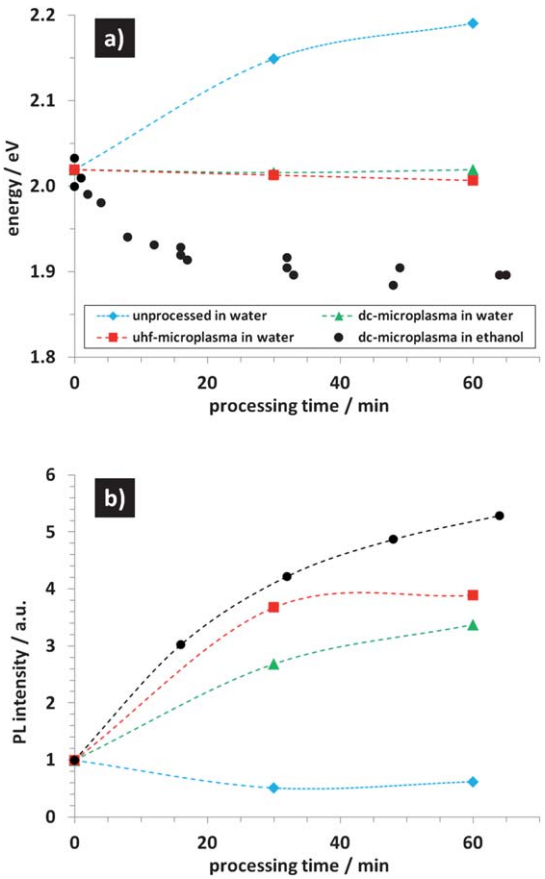

Fig. 5 Photoluminescence (PL) energy (a) and intensity (b) for Si-ncs processed for different times utilizing either a direct-current (dc) microplasma or an ultra high frequency (uhf) microplasma in water or ethanol. PL properties of Si-ncs stored in water for the same time are also reported.

and the loss of PL intensity observed for Si-ncs stored in water (blue diamonds in Fig. 5). The microplasma processes have effectively stopped the inward oxidation observed for the unprocessed Si-ncs so that no blue shift is observed due to the decreasing size of the core (Fig. 5a) and the PL intensity has not decreased due to the introduction of defective sites (Fig. 5b). In contrast, the PL intensity is increased possibly due to a more complete passivation of a higher number of Si-ncs.

Specifically, the PL peak energy of Si-ncs treated by the dc-microplasma in water remains just above 2 eV (~610 nm) and the PL intensity is increased. The analysis of the surface properties by FTIR has revealed in this case very subtle changes in the type and arrangements of the surface Si–O bonds. It is confirmed that a mix of oxidation and H-terminations are still present after the dc-microplasma treatment, however the new surface bonds are qualitatively different. In order to understand in detail the different qualitative nature of surface Si–O bonds, further analysis involving a combination of surface characterization techniques will be required.[84] We are however able to comment on the plasma-induced chemistry as our studies have confirmed that the microplasma–water process produces hydrogen peroxide; H_2O_2 is produced *via* cascaded chemistry initiated by electron-induced reactions at the plasma–water interface.[84,88,98] We therefore believe that H_2O_2 is partly responsible for the surface oxidation of the Si-ncs contributing to remove any surface defects and increasing the PL intensity. Nonetheless, our results also show that H_2O_2 alone cannot improve the surface properties of Si-ncs and therefore a combined effect with other plasma-produced radicals is taking place. Due to a fast kinetically driven reaction chemistry, the plasma-induced oxidation may have produced a stable surface oxide layer that is effectively preventing the oxide from growing inward. It is now interesting to analyse the effect of the uhf-microplasma on the Si-ncs/water colloid. The behaviour of the PL energy with processing time appears to be very similar to the one measured for the colloid processed by a dc-microplasma (Fig. 5a). This trend is justified considering that also in this case we have been able to verify the formation of hydrogen peroxide when water is exposed to the uhf-microplasma jet. Fig. 5b on the other side suggests that the uhf-microplasma may be more efficient in activating the surface chemistry and it is capable of passivating a larger number of Si-ncs before these undergo irreversible degradation due to the low-temperature water-induced oxidation. In the dc-microplasma configuration the possibility of electron losses is minimized as the microplasma is directly coupled to the colloid, while in the uhf-microplasma, electrons produced in the remote plasma have a wide range of possible loss mechanisms before they can reach the liquid surface. Based on these comments and considering that plasma electrons are believed to initiate the reaction chain, the higher efficiency of the uhf-microplasma process is counterintuitive. However it should be noted that the electron density of a high-frequency plasma is generally expected to be much higher than a dc-coupled plasma under these conditions.[31] Furthermore, although water is not directly coupled to the uhf-microplasma, it is highly possible that the water surface behaves as a floating ground which is capable of attracting electrons from the microplasma jet. Therefore, while more in-depth studies are currently in progress, it is not surprising to see the uhf-microplasma to outperform the dc-configuration.

Finally, dc-microplasma processing in ethanol demonstrates that a different type of surface engineering can be achieved by changing the liquid media. We have previously studied the surface characteristics of Si-ncs that were microplasma-treated in ethanol; these have shown that terminations of the Si–O–R type are likely to be formed after the dc-microplasma treatment in ethanol.[87] The different surface chemistry activated in ethanol is believed to be due to different reactions induced by plasma-electrons at the plasma–ethanol interface compared with plasma–water.[87] The Si-nc surface based on Si–O–R produces a considerable PL red-shift of more than 50 nm, *i.e.* a large reduction of the PL energy (>0.1 eV; black circles, Fig. 5a), which is consistent with single-bonded Si–O terminations such as in Si–OH (see also Fig. 1).[33,65] In this type of surface ligand, the Si–O bond is strongly affected by the oxygen electro-negativity without being "averaged" between double bonds as is the case for Si=O and Si–O–Si; double bonds are likely to be found in H_2O_2-induced oxidation (red squares and green triangles in Fig. 5a). Because water-induced oxidation is much slower in ethanol, surface engineering in ethanol is again much more

efficient as more Si-ncs can be passivated before these are irreparably oxidized; this yields a very high PL intensity for Si-ncs treated in ethanol (black circles, Fig. 5b). Although the results are not presented here, uhf-microplasma processing of Si-ncs in ethanol exhibits even higher efficiency in the passivation of the Si-ncs as it was observed when dc- and uhf-microplasma treatments in water were compared (red squares *vs.* green triangles in Fig. 5b).

3.5 Comparison of plasma–liquid surface engineering and comments on oxygen-based chemistry

We would like to point out that while both laser- and microplasma-based processing lead to similar results in some aspects, there appear to be some fundamental differences in the two approaches originating from quite different physics of the respective plasmas. For instance, laser-processing is useful in the fragmentation of Si-nc aggregates and this can be observed in a narrowing of the broad PL peak after laser processing in ethanol (Fig. 4b); this is not observed in Si-ncs processed by microplasma (not shown here). On the other side, microplasma processing leads to much improved PL properties compared to laser processing. The PL intensity of dc-microplasma treated Si-ncs in ethanol can be up to five times higher than laser-processed Si-ncs (also not shown here); it follows that microplasma processing does not affect the size distribution of the Si-ncs and that in this case surface engineering is the only mechanism for tuning the Si-nc optical properties.

The simplicity, flexibility and results demonstrate superior capabilities of the microplasma-based surface engineering approach. This is the result of multiple mechanisms induced by the microplasma process and due to more efficient electron-driven non-equilibrium liquid chemistry.[31,85,87,88,97,108] The chemistry induced at the plasma–liquid interface is still subject of debate in the plasma community, however a range of results are supporting the major contribution of plasma electrons in activating liquid chemistry.[88,98–101] This type of electron-induced chemistry and consequent surface passivation cannot be achieved in the case of ns-laser processing, which remains in any case less efficient. In this context, an important observation is that plasma produced at the surface of the liquid can efficiently inject externally produced electrons from the plasma gas to the colloid. Laser-produced plasma inside the liquid volume can only produce pairs of oppositely charged species which are secluded within the same volume and are therefore more likely to recombine limiting the reaction time with other species. Therefore, radical formation through laser processing follows a different reaction path with a very different thermodynamics compared to microplasma processing. A detailed, in-depth and direct comparison of the chemistries produced by the two different techniques is not currently available; however several studies are indeed available separately in the literature.

We would like to emphasize that the results reported here have highlighted the importance of oxygen-based chemistry at the surface of the Si-ncs. The general perception of Si-nc oxidation is linked to an undesired outcome; we hope that we have here clarified that carefully controlled surface engineering based on oxygen bonds can deliver Si-ncs with useful optical properties which are furthermore highly stable in liquids including water. In addition, the richness of oxygen-based bond configurations can provide a range of opportunities for tuning the Si-nc properties including both optical as well as electronic properties *via* the control of charge transfer mechanisms.

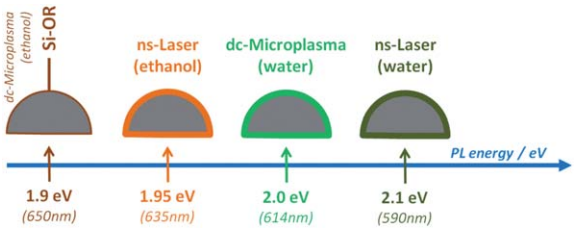

Fig. 6 Schematic diagram depicting the range of oxygen-based surface engineering and their photoluminescence properties.

In Fig. 6 we depict the range of stable Si-ncs with different optical properties that exhibit emission from 590 nm up to 650 nm just by varying the oxygen-bonding configuration at the surface. The microplasma-treated Si-ncs in ethanol (left) are the ones that produce the highest PL intensity. Although there is no obvious correlation the most-right Si-ncs in Fig. 6 are the ones that have the weakest PL intensity.

4 Conclusions and application outlook

Surface engineering of Si-ncs has seen considerable progress both theoretically and experimentally. Aspects that are related to the interplay between quantum confinement and surface effects have been clearly identified. However, major gaps between theoretical results and experimental evidence still need to be overcome in order to provide a coherent understanding of Si-nc behaviour and properties. It is obvious that static calculation of energy structures is not sufficient to describe the complex nature of indirect semiconductor nanocrystals and transition dynamics needs to be considered to have an appreciation of Si-nc behaviour.

The employment of Si-ncs in a range of applications also requires careful investigation on the surface conditions of Si-ncs, which implies that both theoretical studies and experimental endeavours have to master the surface description for Si-ncs in the diameter range 1–5 nm. Furthermore, charge transfer at the interface is an aspect that requires urgent attention. From a theoretical point of view, the abstraction to an ideal stand-alone Si-nc may need to be upgraded to an application-oriented integrated Si-nc. Experimentally, in addition to achieving accurate control of surface characteristics, advances are also needed in characterization approaches with theoretical efforts to model how an analytical tool interacts with Si-nc ensembles and how meaningful information could be extracted.

Measurement techniques that can assess the functionalities of the Si-nc interface need to be developed so that the charge transfer and dissociation mechanisms can be fully understood for a range of surface conditions. This is because interfaces are

the key to Si-nc applications. For instance, the fundamental aspects of exciton dissociation are highly important to improve the efficiency of solar cells based on quantum dots. Similarly, interfaces are at the basis of application in water splitting, they require to be controlled for bio-imaging and may open up great opportunities for the development of most advanced technologies in autonomous nano-engines.

Microplasmas and laser-based surface engineering have shown the capabilities to support the required experimental efforts to achieve important scientific objectives as described above. At this stage the industrial scalability of these processes does not represent a limiting factor. Nonetheless it should be noted that both laser-based processes and microplasma technology have demonstrated the potential for scaled-up configurations[31,109,110] to achieve large scale surface engineering as would be required for applications such as photovoltaics.

Acknowledgements

The authors would like to acknowledge the support of NEDO (Japan). DM is thankful to the University of Ulster Strategic Research Fund and to the JSPS Bridge Fellowship. Finally SM thanks the financial support of the University of Ulster Vice-Chancellor Studentship.

References

1 R. F. Service, *Science*, 2008, **322**, 1784.
2 M. Howarth, W. Liu, S. Puthenveetil, Y. Zheng, L. F. Marshall, M. M. Schmidt, K. D. Wittrup, M. G. Bawendi and A. Y. Ting, *Nat. Methods*, 2008, **5**, 397–399.
3 M. E. Åkerman, W. C. W. Chan, P. Laakkonen, S. N. Bhatia and E. Ruoslahti, *Proc. Natl. Acad. Sci. U. S. A.*, 2002, **99**, 12617–12621.
4 X. Michalet, F. F. Pinaud, L. A. Bentolila, J. M. Tsay, S. Doose, J. J. Li, G. Sundaresan, A. M. Wu, S. S. Gambhir and S. Weiss, *Science*, 2005, **307**, 538–544.
5 D. Kovalev, H. Heckler, G. Polisski and F. Koch, *Phys. Status Solidi B*, 1999, **215**, 871–932.
6 K. Hyeon-Deuk and O. V. Prezhdo, *ACS Nano*, 2012, **6**, 1239–1250.
7 C. Delerue and M. Lannoo, *Nanostructures: Theory and Modelling*, Springer, 2004, ISBN 3-540-20694-9.
8 C. B. Murray, D. J. Norris and M. G. Bawendi, *J. Am. Chem. Soc.*, 1993, **115**, 8706–8715.
9 Z. A. Peng and X. Peng, *J. Am. Chem. Soc.*, 2001, **123**, 183–184.
10 R. D. Schaller and V. I. Klimov, *Phys. Rev. Lett.*, 2004, **92**, 186601.
11 O. E. Semonin, J. M. Luther, S. Choi, H.-Y. Chen, J. Gao, A. J. Nozik and M. C. Beard, *Science*, 2011, **334**, 1530–1533.
12 F. A. Reboredo and G. Galli, *J. Phys. Chem. B*, 2005, **109**, 1072–1078.
13 M. J. L. Portoles, R. P. Diez, M. L. Dell'Arciprete, P. Caregnato, J. J. Romero, D. O. Martire, O. Azzaroni, M. Ceolín and M. C. Gonzalez, *J. Phys. Chem. C*, 2012, **116**, 11315–11325.
14 S. Tiwari, F. Rana, H. Hanafi, A. Hartstein, E. F. Crabbe and K. Chan, *Appl. Phys. Lett.*, 1996, **68**, 1377–1379.
15 D. Timmerman, I. Izeddin, P. Stallinga, I. N. Yassievich and T. Gregorkiewicz, *Nat. Photonics*, 2008, **2**, 105–109.
16 C.-Y. Liu, Z. C. Holman and U. R. Kortshagen, *Adv. Funct. Mater.*, 2010, **20**, 2157–2164.
17 G. Uchida, K. Yamamoto, M. Sato, Y. Kawashima, K. Nakahara, K. Kamataki, N. Itagaki, K. Koga and M. Shiratani, *Jpn. J. Appl. Phys.*, 2012, **51**, 01AD01.
18 C.-Y. Liu, Z. C. Holman and U. R. Kortshagen, *Nano Lett.*, 2009, **9**, 449–452.
19 V. Švrček and D. Mariotti, *Pure Appl. Chem.*, 2012, **84**, 2629–2639.
20 V. Švrček, T. Yamanari, D. Mariotti, K. Matsubara and M. Kondo, *Appl. Phys. Lett.*, 2012, **100**, 223904.
21 V. Švrček, D. Mariotti, T. Nagai, Y. Shibata, I. Turkevych and M. Kondo, *J. Phys. Chem. C*, 2011, **115**, 5084–5093.
22 V. Švrček, D. Mariotti, Y. Shibata and M. Kondo, *J. Phys. D: Appl. Phys.*, 2010, **43**, 415402.
23 R. J. Anthony, K.-Y. Cheng, Z. C. Holman, R. J. Holmes and U. R. Kortshagen, *Nano Lett.*, 2012, **12**, 2822–2825.
24 C. Huh, C.-J. Choi, W. Kim, B. K. Kim, B.-J. Park, E.-H. Jang, S.-H. Kim and G. Y. Sung, *Appl. Phys. Lett.*, 2012, **100**, 181108.
25 Y.-M. Lin, K. C. Klavetter, P. R. Abel, N. C. Davy, J. L. Snider, A. Helier and C. B. Mullins, *Chem. Commun.*, 2012, **48**, 7268–7270.
26 A. Gohier, B. Laïk, K.-H. Kim, J.-L. Maurice, J.-P. Pereira-Ramos, C. S. Cojocaru and P. T. Van, *Adv. Mater.*, 2012, **24**, 2592–2597.
27 D. Kovalev and M. Fujii, *Adv. Mater.*, 2005, **17**, 2531–2544.
28 Z. F. Li and E. Ruckenstein, *Nano Lett.*, 2004, **4**, 1463–1467.
29 A. Gupta, M. T. Swihart and H. Wiggers, *Adv. Funct. Mater.*, 2009, **19**, 696–703.
30 O. Yasar-Inceoglu, T. Lopez, E. Farshihagro and L. Mangolini, *Nanotechnology*, 2012, **23**, 255604.
31 D. Mariotti and R. M. Sankaran, *J. Phys. D: Appl. Phys.*, 2010, **43**, 323001.
32 T. M. Atkins, A. Y. Louie and S. M. Kauzlarich, *Nanotechnology*, 2012, **23**, 294006.
33 I. E. Anderson, R. A. Shircliff, C. Macauley, D. K. Smith, B. G. Lee, S. Agarwal, P. Stradins and R. T. Collins, *J. Phys. Chem. C*, 2012, **116**, 3979–3987.
34 V. Švrček, D. Mariotti and M. Kondo, *Opt. Express*, 2009, **17**, 520–527.
35 M. L. Mastronardi, E. J. Henderson, D. P. Puzzo and G. A. Ozin, *Adv. Mater.*, 2012, **24**, 5890–5898.
36 Q. Cheng, E. Tam, S. Xu and K. K. Ostrikov, *Nanoscale*, 2012, **2**, 594–600.
37 T. Nakamura, S. Adachi, M. Fujii, K. Miura and S. Yamamoto, *Phys. Rev. B: Condens. Matter Mater. Phys.*, 2012, **85**, 045441.
38 I. Sychugov, J. Valenta, K. Mitsuishi and J. Linnros, *Phys. Rev. B: Condens. Matter Mater. Phys.*, 2012, **86**, 075311.

39 A. Carvalho, S. Öberg, M. Barroso, M. J. Rayson and P. Briddon, *Phys. Status Solidi A*, 2012, **209**, 1847–1850.
40 H. Sugimoto, M. Fujii, K. Imakita, S. Hayashi and K. Akamatsu, *J. Phys. Chem. C*, 2012, **116**, 17969–17974.
41 H. Sugimoto, M. Fujii, M. Fukuda, K. Imakita and S. Hayashi, *J. Appl. Phys.*, 2011, **110**, 063528.
42 S. A. Fischer and O. V. Prezhdo, *J. Phys. Chem. C*, 2011, **115**, 10006–10011.
43 F. Ioria and S. Ossicini, *Phys. E*, 2009, **41**, 939–946.
44 M. Ito, K. Imakita, M. Fujii and S. Hayashi, *J. Phys. D: Appl.Phys.*, 2010, **43**, 505101.
45 X. Pi, X. Chen and D. Yang, *J. Phys. Chem. C*, 2011, **115**, 9838–9843.
46 X. Pi, X. Chen, Y. Ma and D. Yang, *Nanoscale*, 2011, **3**, 4584–4588.
47 F. Erogbogbo, C.-W. Chang, J. May, P. N. Prasad and M. T. Swihart, *Nanoscale*, 2012, **4**, 5163–5168.
48 C.-Y. Liu and U. R. Kortshagen, *Nanoscale*, 2012, **4**, 3963–3968.
49 I. Levchenko, K. Ostrikov, D. Mariotti and V. Švrček, *Carbon*, 2009, **47**, 2379–2390.
50 K. Kůsová, L. Ondič, E. Klimešová, K. Herynková, I. Pelant, S. Daniš, J. Valenta, M. Gallart, M. Ziegler, B. Hönerlage and P. Gilliot, *Appl. Phys. Lett.*, 2012, **101**, 143101.
51 B. D. Rezgui, F. Gourbilleau, D. Maestre, O. Palais, A. Sibai, M. Lemiti and G. Brémond, *J. Appl. Phys.*, 2012, **112**, 024324.
52 J. Heitmann, F. Müller, M. Zacharias and U. Gösele, *Adv. Mater.*, 2005, **17**, 795–803.
53 R. Guerra, E. Degoli and S. Ossicini, *Phys. Rev. B: Condens. Matter Mater. Phys.*, 2009, **80**, 155332.
54 W. D. A. M. de Boer, D. Timmerman, K. Dohnalova, I. N. Yassievich, H. Zhang, W. J. Buma and T. Gregorkiewicz, *Nat. Nanotechnol.*, 2010, **5**, 878–884.
55 F. Trojánek, K. Neudert, P. Malý, K. Dohnalová and I. Pelant, *J. Appl. Phys.*, 2006, **99**, 116108.
56 A. Gali, M. Vörös, D. Rocca, G. T. Zimanyi and G. Galli, *Nano Lett.*, 2009, **9**, 3780–3785.
57 M. C. Beard, K. P. Knutsen, P. Yu, J. M. Luther, Q. Song, W. K. Metzger, R. J. Ellingson and A. J. Nozik, *Nano Lett.*, 2007, **7**, 2506–2512.
58 A. J. Nozik, *Phys. E*, 2002, **14**, 115–120.
59 J. M. Buriak, *Chem. Rev.*, 2002, **102**, 1271–1308.
60 M. E. Ahmed, J. P. Goss, R. J. Eyre, P. R. Briddon and M. A. Taylforth, *J. Phys.: Conf. Ser.*, 2010, **245**, 012046.
61 Y. Kanemitsu, H. Uto, Y. Masumoto, T. Masumoto, T. Futagi and H. Mimura, *Phys. Rev. B: Condens. Matter Mater. Phys.*, 1993, **48**, 2827–2831.
62 M. V. Wolkin, J. Jorne, P. M. Fauchet, G. Allan and C. Delerue, *Phys. Rev. Lett.*, 1999, **82**, 197–200.
63 P. Carrier, *Phys. Rev. B: Condens. Matter Mater. Phys.*, 2009, **80**, 075319.
64 F. Meinardi and A. Paleari, *Phys. Rev. B: Condens. Matter Mater. Phys.*, 1998, **58**, 3511–3514.
65 D. König, J. Rudd, G. Conibeer and M. A. Green, *Mater. Sci. Eng., B*, 2009, **159–160**, 117–121.
66 S. Kim, M. C. Kim, S.-H. Choi, K. J. Kim, H. N. Hwang and C. C. Hwang, *Appl. Phys. Lett.*, 2007, **91**, 103113.
67 Y. Tu and J. Tersoff, *Phys. Rev. Lett.*, 2000, **84**, 4393–4396.
68 L. E. Ramos, J. Furthmüller and F. Bechstedt, *Phys. Rev. B: Condens. Matter Mater. Phys.*, 2004, **70**, 033311.
69 R. Guerra, M. Ippolito, S. Meloni and S. Ossicini, *Appl. Phys. Lett.*, 2012, **100**, 181905.
70 G. Conibeer, M. Green, E.-C. Cho, D. König, Y.-H. Cho, T. Fangsuwannarak, G. Scardera, E. Pink, Y. Huang, T. Puzzer, S. Huang, D. Song, C. Flynn, S. Park, X. Hao and D. Mansfield, *Thin Solid Films*, 2008, **516**, 6748–6756.
71 E. Ramos, B. M. Monroy, J. C. Alonso, L. E. Sansores, R. Salcedo and A. Martínez, *J. Phys. Chem. C*, 2012, **116**, 3988–3994.
72 U. Kortshagen, *J. Phys. D: Appl. Phys.*, 2009, **42**, 113001.
73 R. K. Baldwin, K. A. Pettigrew, E. Ratai, M. P. Augustine and S. M. Kauzlarich, *Chem. Commun.*, 2002, 1822–1823.
74 R. Gresback, T. Nozaki and K. Okazaki, *Nanotechnology*, 2011, **22**, 305605.
75 J. Wang, Y. Liu, F. Peng, C. Chen, Y. He, H. Ma, L. Cao and S. Sun, *Small*, 2012, **8**, 2430–2435.
76 N. Prtljaga, E. D'Amato, A. Pitanti, R. Guider, E. Froner, S. Larcheri, M. Scarpa and L. Pavesi, *Nanotechnology*, 2011, **22**, 215704.
77 Y. Zhong, F. Peng, X. Wei, Y. Zhou, J. Wang, X. Jiang, Y. Su, S. Su, S.-T. Lee and Y. He, *Angew. Chem., Int. Ed.*, 2012, **51**, 8485–8489.
78 E. V. Rogozhina, D. A. Eckhoff, E. Gratton and P. V. Braun, *J. Mater. Chem.*, 2006, **16**, 1421–1430.
79 A. K. Mandal, M. Ray, I. Rajapaksa, S. Mukherjee and A. Datta, *J. Phys. Chem. C*, 2012, **116**, 14644–14649.
80 S. Niesar, R. N. Pereira, A. R. Stegner, N. Erhard, M. Hoeb, A. Baumer, H. Wiggers, M. S. Brandt and M. Stutzmann, *Adv. Funct. Mater.*, 2012, **22**, 1190–1198.
81 J. M. Buriak, M. P. Stewart, T. W. Geders, M. J. Allen, H. C. Choi, J. Smith, D. Raftery and L. T. Canham, *J. Am. Chem. Soc.*, 1999, **121**, 11491–11502.
82 S. Alkis, A. K. Okyay and B. Ortaç, *J. Phys. Chem. C*, 2012, **116**, 3432–3436.
83 R. J. Anthony, D. J. Rowe, M. Stein, J. Yang and U. Kortshagen, *Adv. Funct. Mater.*, 2011, **21**, 4042–4046.
84 S. Mitra, V. Švrček, D. Mariotti, K. Matsubara and M. Kondo, in preparation.
85 V. Švrček, D. Mariotti and M. Kondo, *Appl. Phys. Lett.*, 2010, **97**, 161502.
86 J. McKenna, J. Patel, S. Mitra, N. Soin, V. Švrček and D. Mariotti, *Eur. Phys. J.: Appl. Phys.*, 2011, **56**, 24020.
87 D. Mariotti, V. Švrček, J. W. J. Hamilton, M. Schmidt and M. Kondo, *Adv. Funct. Mater.*, 2012, **22**, 954–964.
88 D. Mariotti, J. Patel, V. Švrček and P. Maguire, *Plasma Processes Polym.*, 2012, **9**, 1074–1085.
89 N. Salivati, N. Shuall, J. M. McCrate and J. G. Ekerdt, *J. Phys. Chem. Lett.*, 2010, **1**, 1957–1961.
90 X. Wang, R. E. Ruther, J. A. Streifer and R. J. Hamers, *J. Am. Chem. Soc.*, 2010, **132**, 4048–4049.
91 L. Mangolini and U. Kortshagen, *Adv. Mater.*, 2007, **19**, 2513–2519.

92 W.-H. Chiang and R. M. Sankaran, *Nat. Mater.*, 2009, **8**, 882–886.
93 Y.-C. Liao and J. T. Roberts, *J. Am. Chem. Soc.*, 2006, **128**, 9061–9065.
94 K. K. Ostrikov, I. Levchenko, U. Cvelbar, M. Sunkara and M. Mozetic, *Nanoscale*, 2012, **2**, 2012–2027.
95 V. Švrček, M. Kondo, K. Kalia and D. Mariotti, *Chem. Phys. Lett.*, 2009, **478**, 224.
96 J. Fendler, *Chem. Mater.*, 2001, **13**, 3196–3210.
97 D. Mariotti and R. M. Sankaran, *J. Phys. D: Appl. Phys.*, 2011, **44**, 174023.
98 J. Patel, L. Němcová, P. Maguire, W. G. Graham and D. Mariotti, *Adv. Funct. Mater.*, submitted.
99 C. Richmonds, M. Witzke, B. Bartling, S. W. Lee, J. Wainright, C.-C. Liu and R. M. Sankaran, *J. Am. Chem. Soc.*, 2011, **44**, 17582–17585.
100 M. Witzke, P. Rumbach, D. B. Go and R. M. Sankaran, *J. Phys. D: Appl. Phys.*, 2012, **45**, 442001.
101 S. W. Lee, D. Liang, X. P. A. Gao and R. M. Sankaran, *Adv. Funct. Mater.*, 2011, **21**, 2155–2161.
102 V. Švrček, D. Mariotti, K. Matsubara and M. Kondo, *Rev. Laser Eng.*, 2012, **40**, 1–5.
103 K. Ostrikov, U. Cvelbar and A. B. Murphy, *J. Phys. D: Appl. Phys.*, 2011, **44**, 174001.
104 T. Nozaki, V. Goujard, S. Yuzawa, S. Moriyama, A. Agıral and K. Okazaki, *J. Phys. D: Appl. Phys.*, 2011, **44**, 274010.
105 V. Švrček, A. Slaoui and J.-C. Muller, *J. Appl. Phys.*, 2004, **95**, 3158–3163.
106 V. Švrček, *Pure Appl. Chem.*, 2010, **82**, 2121–2135.
107 Y. H. Ogata, F. Kato, T. Tsuboi and T. Sakka, *J. Electrochem. Soc.*, 1998, **145**, 2439–2444.
108 B. H. Milosavljevic and O. I. Micic, *J. Phys. Chem.*, 1978, **82**, 1359–1362.
109 M. K. Kulsreshath, L. Schwaederle, L. J. Overzet, P. Lefaucheux, J. Ladroue, T. Tillocher, O. Aubry, M. Woytasik, G. Schelcher and R. Dussart, *J. Phys. D: Appl. Phys.*, 2012, **45**, 285202.
110 J. Y. Kim, J. Ballato and S.-O. Kim, *Plasma Processes Polym.*, 2012, **9**, 253–260.

